Current Trends in Biotechnology and Pharmacy
Vol. 17(Supplementary issue - 3A)1116 - 1128, August 2023, ISSN 0973-8916 (Print), 2230-7303 (Online)
10.5530/ctbp.2023.3s.50

Synthesis, Characterization and Antimicrobial Studies of Gabapentin Schiff Base Metal Complexes Containing Heterocyclic Ligand via Microwave-Assisted Method

Jyoti C Ajbani[1], D Smita Revankar[1],M. Revanasiddappa[1]*, Suresh Babu Naidu Krishna[2], S Shankara[3]

[1]Department of Engineering Chemistry, PESIT, Bangalore South campus, Bangalore, Karnataka, India, 560 100
[2]Department of Biomedical and Clinical Technology, Durban University of Technology, Durban, South Africa – 4000
[3]Department of Microbiology, Government Science College, Nrupathunga University, Bangalore, Karnataka

Corresponding author: revanasiddappam@pes.edu

Abstract

The use of microwave-assisted synthesis in the formation of coordination metal complexes has led to improved control of waste generation and reduced reaction times. In the present study, new Schiff base metal complexes of various metals, including ZrO (II), VO(II), Cr (III), Mn (II), Fe (II), Co (II), Ni (II), Cu (II), Zn (II), Cd (II), and Hg (II), were synthesized using microwave radiation.To characterize the synthesized metal complexes, several physical methods were used, including elemental analysis, FT-IR, molar conductance, electronic spectra, 1H-NMR, ESR, magnetic susceptibility, thermal, electrical conductivity, and XRD analysis. Elemental analysis revealed that the complexes were of the 1:1, 1:2, and 1:3 (M: L) types. The observed molar conductance values indicated that the complexes were non-electrolytes. The 1H-NMR spectral data suggested that the phenolic protons had been displaced during complexation. Thermo gravimetric analysis showed the presence of water molecules in the coordination metal complexes and confirmed the loss of water molecules in the first step, followed by the decomposition of the ligand in the subsequent step. The synthesized ligand and coordination metal complexes were also studied for their antibacterial and antifungal activity. They were tested against various bacteria and fungi, including *Escherichia coli, Salmonella enteric, klebsiella pneumoniae, Staphylococcus aureus, Streptococcus agalactiae, Aspergillus niger,* and *Aspergillus flavu*s. The results indicated that some of the metal complexes showed significant antibacterial and antifungal activity. Overall, the use of microwave-assisted synthesis in the formation of coordination metal complexes has led to the synthesis of new metal complexes with potential antibacterial and antifungal activity. The various physical methods used for characterization have provided valuable insights into the properties and behaviour of these metal complexes.

Keywords: Microwave method; Heterocyclic ligand; Thermal study.

Introduction

Extensive studies have been conducted on Schiff bases derived from amide and aldehyde, which are an important class of ligands that coordinate with metal ions through azomethine nitrogen [1-4]. These complexes play a pivotal role in the development of coordination chemistry [5-8]. Gabapentin derivatives have been found to have numerous uses in medicinal and pharmaceutical fields [9-11]. The compounds were evaluated for their anticonvulsant and

Vol. 17(Supplementary issue - 3A)1116 - 1128, August 2023, ISSN 0973-8916 (Print), 2230-7303 (Online)
10.5530/ctbp.2023.3s.50

antioxidant activities using the Maximal Electroshock Seizure (MES) test. The majority of the compounds showed activity in the MES tests.

Schiff bases have also found applications in analytical chemistry where some compounds were used as a ligand to prepare complexes and catalysts and as a corrosion inhibitor in the chemical industry [12]. Microwave irradiation has gained popularity as it accelerates the reaction rate in a solvent-free condition without the use of supporting reagents, making it eco--friendly. Chemical transformations that took hours or even days to complete the reaction can be completed in minutes with microwave irradiation. Microwave irradiation offers numerous benefits, including higher yields, shorter reaction times, and eco-friendly and simple reaction conditions [13-17]. Therefore, the aim of this work is to synthesize and characterize new transition metal complexes of Schiff bases derived from Gabapentin with aldehydes using microwave-assisted synthesis and to screen their antibacterial activity

Materials and Methods

All reagents used were of analytical grade. Metal chlorides were procured from Sigma Aldrich, India and used as received. The drug molecules were purchased from Apotecx Pharma Chem India Ltd. All solvents were distilled prior to use.

Synthesis of schiff base ligand gabapantin - 2-hydroxy naphthaldehyde

The Synthesis of Schiff base ligand Gabapantin - 2-hydroxy naphthaldehyde as shown in the figure 1. Gabapentin (0.03M, 0.51g) was added to a dry and clean round bottom flask and dissolved in 5-7ml of methanol. To this, 2-hydroxy naphthaldehyde (0.03M, 0.54g) was added. The mixture was placed in a round bottom flask and capped with a water condenser before being subjected to microwave irradiation at 10% intensity (110 watts) for 1 minute with a pulse of 30 seconds. The progress of the reaction was monitored using TLC. Once the reaction was complete, the mixture was cooled to room temperature. The Schiff base was then separated, filtered using Whatman filter paper, washed with hot methanol, and kept for re-crystallization. The resulting yellow crystals were separated by drying and stored in a desiccator.

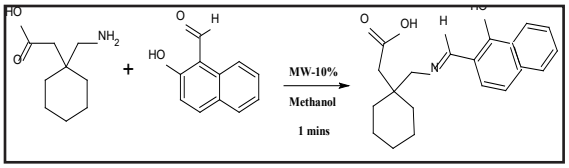

Gabapentin 2-hydroxynaphthaldehydeSchiff base ligand

Figure- 1 Scheme for synthesis of Schiff base ligand(HL)$C_{16}H_{11}O_3N_2F_3S$ [RO]: Mol. wt. 368.247, m.p. 108-1100C, yield 89.58%

Synthesis of metal complexes

Metal complexes were synthesized by irradiating equimolar ratio of hydrated metal chlorides and ligand in ethanol (1-2ml) as a solvent with a pinch of sodium acetate was added to initiate the precipitation. Solid was separated out, filtered and washed with distilled water, recrystallized from ethyl alcohol. All complexes were dried in air and kept over anhydrous calcium chloride in the desiccator. Formation of the complexes may be represented as follows:

$$MCl_2.nH_2O + HL \xrightarrow{\text{ethanol, NaOAC, Metal complex 8-10 minutes in MW}} ML_{n=1,2.}(H_2O)_{n=0,1,2}\,Cl_{n=0,1}$$

Metal salt Ligand 30% intensity

Where, M=Cu (II), Co (II), Ni (II), Mn(II),Fe(III),Zn(II),Hg(II),Cd(II),Cr(III),ZrO(II),VO(II).

Physical measurements

Inductively Coupled Plasma-Optical Emission Spectrometer, Perkin Elmer-Optima7000DV: This technique is used for the quantitative determination of metals in a sample by measuring the intensity of emitted light from the excited atoms. It provides information about the elemental composition of the complex. SEM-EDX analysis, the complexes were analysed using a Carl Zeiss EVO-18 model SEM coupled with an EDX detector. SEM provides

Vol. 17(Supplementary issue - 3A)1116 - 1128, August 2023, ISSN 0973-8916 (Print), 2230-7303 (Online)
10.5530/ctbp.2023.3s.50

high-resolution images of the sample surface, while EDX determines the elemental composition of the complex by analyzing characteristic X-rays emitted from the sample. Microanalytical analysis of the complexes for carbon, hydrogen, and nitrogen (CHN) as well as sulfur (S) content was carried out using an Elementar Vario EL III model instrument. This technique provides information about the organic constituents present in the complexes. The chloride content in the complexes was determined using the argentometric method. This method involves the titration of chloride ions with silver nitrate, and the end point is detected using a silver indicator. The magnetic susceptibility of the complexes was measured at room temperature using a Gouy balance. The calibrant used was $Hg[Co(NCS)_4]$, and diamagnetic corrections were made using PASCAL's constants. Conductance measurements of the complexes were carried out using an Elico Conductivity bridge. The measurements were performed in DMSO (dimethyl sulfoxide) using a dip-type conductivity cell fitted with platinum electrodes. The conductance value provides information about the ionic behaviour of the complexes. The infrared spectra of the ligands and their complexes were recorded using a Thermo Nicolet Avatar 370 FT-IR spectrophotometer. The spectra were obtained by analyzing the absorption of infrared radiation by the sample in the 4000 to 400 cm-1 range. KBr discs were used as the sample matrix. The nuclear magnetic resonance spectra of the complexes were recorded in DMSO-d6 solvent on a Varian AS 400 MHz spectrophotometer. TMS (tetramethylsilane) was used as the internal standard for chemical shift referencing. The electronic spectra of the complexes were recorded using an Elico-SL-164 double beam UV-visible spectrophotometer. The measurements were performed in DMSO solution at a concentration of 10^{-3} M, and the range of analysis was 200 to 1100 nm. Powder X-ray diffraction analysis of the complexes was carried out using a Bruker AXS D8 Advance instrument. The X-ray source used was Cu with a wavelength of 1.5406 Å. This technique provides information about the crystal structure and phase composition of the complexes. These analytical techniques were employed to characterize and determine the metal content, elemental composition, structural properties, and spectroscopic features of the complexes under investigation.

Antimicrobial activities

The in-vitro antimicrobial activity of the Schiff bases and their complexes was tested against *Escherichia coli, Salmonella enteric, Klebsiella pneumoniae, Staphylococcus aureus, Streptococcus agalactiae, Aspergillus niger,* and *Aspergillus flavus* using the well diffusion method. Muller Hinton agar (MHA) and Potato dextrose agar (PDA) were used as the culture media, and streptomycin and fluconazole were used as control drugs. All complexes were dissolved in DMSO, and separate solutions with a concentration of 100 ppm were prepared.

For the bacterial assay, wells were made on MHA plates inoculated with bacteria. Each well was filled with 100 µl of the test solutions. The bacterial plates were then incubated at 37°C overnight, and the zone of growth inhibition was measured in millimetres. For the fungal assay, wells were made on PDA plates inoculated with fungi. Again, 100 µl of the test solutions were added to each well. The fungal plates were incubated at 27°C for 24-48 hours, and the zone of growth inhibition was measured in millimetres. These measurements were conducted following the referenced sources [18-20].

Results and Discussion

Electronic spectral studies and magnetic properties

The melting points and elemental analyses of both the ligand and its metal complexes are presented in Table 1. It is noteworthy that the calculated values closely matched the experimental values, indicating a high level of agreement between the two sets of data. This suggests that the calculations were reliable and accurate. In the case of microwave-assisted synthesis, it was observed that the reaction could be completed within a shorter timeframe

Vol. 17(Supplementary issue - 3A)1116 - 1128, August 2023, ISSN 0973-8916 (Print), 2230-7303 (Online)
10.5530/ctbp.2023.3s.50

compared to the conventional method. Additionally, higher yields were obtained using the microwave-assisted approach. These observations highlight the efficiency and effectiveness of microwave irradiation as a method for synthesizing the ligand and its metal complexes. Through the analysis of spectral and analytical data, it was determined that all the metal complexes exhibited a 1:2 (metal: ligand) stoichiometry, except for the Zn (II), Cd (II), and Hg (II) complexes, which displayed a 1:1 (metal:ligand) stoichiometry. This difference in stoichiometry suggests distinct coordination modes or binding patterns for these specific metal ions. The molar conductance values of the complexes dissolved in dimethylformamide (DMF) were found to range from 4.69 to 16.5 $ohm^{-1}mole^{-1}cm^2$. These values indicate relatively low molar conductivities, implying that the complexes do not exhibit significant electrolytic behaviour in solution. Therefore, the experimental observations and data discussed provide valuable insights into the properties and characteristics of both the ligand and its metal complexes, shedding light on their structural features and behaviour.

Table 1- Analytical data of ligand and its metal complexes

Ligand/ complexes	Analysis (%), Found (calculated)						Color	Formula weight	% Yield	Melting Point (°C)	Meff (BM)	Molar Conductance $\Omega^{-1}Cm2Mol^{-2}$
	C	H	O	N	Cl	M						
Ligand(H_2L^4)	73.36 (73.82	6.95 (7.12)	14.25 14.75)	4.22 (4.33)	-------	-------	Yellow	325.394	94.58	230	-------	3.21
$[Cr(L^4)_2(H_2O)\ Cl]$	59.98 (59.47)	5.66 (5.99)	15.47 (15.85)	3.7 (3.47)	8.55 (8.79)	12.32 (12.87)	Green	807.772	96.82	>310(NM)	3.75	5.12
[Fe(L4)2(H2O) Cl]	59.33 (59.19)	5.64 (5.96)	15.27 (15.77)	3.87 (3.45)	8.95 (8.75)	13.36 (13.76)	Brown	811.621	97.2	>192(D)	5.88	21.7
$[Co_2(L^4)_2(H_2O)_2]$	59.49 (59.85)	6.87 (6.03)	15.28 (15.94)	3.72 (3.49)	-------	7.28 (7.34)	Light brown	802.632	75.9	>200(D)	4.18	6.23
$[Cu_2(L^4)_2(H_2O)_2]$	59.89 (59.17)	5.87 (5.96)	15.30 (15.76)	3.04 (3.45)	-------	15.02 (15.65)	Pale Green	811.872	96.16	>250(NM)	1.58	4.98
$[Mn_2\ (L^4)_2(H_2O)_2]$	60.68 (60.45)	6.54 (6.09)	16.61 (16.11)	3.45 (3.52)	-------	6.98 (6.91)	Yellow	794.652	94.8	216	5.4	3.49
$[Ni_2\ (L^4)_2(H_2O)_2]$	59.47 (59.89)	6.77 (6.03)	16.02 (15.95)	3.43 (3.49)	-------	7.56 (7.31)	Yellow green	802.152	92.5	>240(D)	2.67	4.45
$[Zn(L^4)(H_2O)]$	59.04 (58.90)	5.37 (5.93)	15.21 (15.69)	6.61 (6.87)	-------	16.61 (16.03)	Pale yellow	407.796	87.14	192	Dia	5.79
$[Cd(L^4)(H_2O)]$	52.54 (52.81)	5.58 (5.32)	14.24 (14.07)	3.24 (3.08)	-------	24.31 (24.71)	Pale yellow	454.796	88.57	230(D)	Dia	12.24
$[Hg(L^4)(H_2O)]$	44.87 (44.23)	4.94 (4.45)	11.27 (11.79)	2.15 (2.58)	-------	36.22 (36.94)	Yellow	542.976	81.5	226	Dia	4.19
$[ZrO(L^4)(H_2O)]$	53.84 (53.42)	5.03 (5.38)	10.25 (10.68)	3.45 (3.12)	-------	20.01 (20.29)	Yellow	449.606	97.4	212	Dia	11.16
$[VO(L^4)(H_2O)]$	58.93 (58.68)	5.53 (5.91)	11.42 (11.73)	3.99 (3.42)	-------	12.99 (12.44)	Dirty green	409.326	78.6	>200(D)	1.8	12.54

The magnetic moments of the metal complexes are listed in Table 1. The Fe-complex exhibited a magnetic moment of 5.88 BM (Bohr magneton) with 5 unpaired electrons. This magnetic susceptibility value for Fe (II) is consistent with the reported values and indicates a coordination number of six, corresponding to an octahedral geometry. For the Co (II) complexes, the magnetic moments were found to be 4.18 BM, suggesting a high spin complex with octahedral geometry [21-22].

The Ni (II) complex exhibited a magnetic moment value of 2.67 BM, which is close to the expected value for octahedral complexes. This further supports the presence of an octahedral geometry for the Ni (II) complex. The Cu (II) complex displayed a magnetic moment value of 1.58 BM, confirming the distorted octahedral geometry around the copper ion [23]. Electronic spectral studies were conducted using a DMSO solution ($1x10^{-3}M$) for the paramagnetic complexes. The EPR spectral data of all the paramagnetic complexes are presented in Table 2.

For the Ni (II) complex with a coordination number of 6, bands at 14647.722 cm^{-1} and 23474.18 cm^{-1} were observed, corresponding to $3A_2g\ (F) \rightarrow 3T_1g\ (F)$ (v2) and $3A_2g\ (F) \rightarrow 3T_1g\ (P)$(v3) transitions, respectively, in an octahedral environment. The band for the transition $3A_2g\ (F) \rightarrow 3T_2g\ (F)$ (v1) could not be observed due to limitations in the instrument. However, its value can be calculated using a band fitting procedure. Other studies have reported four absorption bands for the Ni (II) complex in the

range of 390, 664, 740 and 1132 nm in the solid state [24]. The Co (II) complex of H2L4 exhibited two bands at 18903 cm^{-1} and 22679 cm^{-1}, which are assigned to the $4T_1g$ F)→$4T_2g$ (F) (v1), $4T_1g$(F)→$4A_2g$ (F) (v2), and $4T_1g$(F)→$4T_1g$ (P) (v3) transitions, respectively. The calculation of $4T_1g$ (F)→$4T_2g$ (F) (v1) was performed using a band procedure, suggesting an octahedral geometry for the Co (II) complex [26].

In the Cu (II) complex of H_2L_4, a broad absorption band with low energy was observed at 15479.2 cm^{-1}, indicating a d-d transition and suggesting a low C2V symmetry of the Cu^{2+} ion. Another band around 27467.2 cm^{-1} (364 nm) can be assigned to M→L charge transfer and π→π* transition associated with the azomethine linkage. Other authors have also reported the region of 540-720 nm for oxo-bridged Cu (II) complexes. Considering all these observations, the presence of the band at 540 nm in the current copper (II) complex indicates a square pyramidal geometry [27]. The aforementioned experimental data provide valuable insights into the magnetic properties and coordination geometries of the metal complexes studied. The electronic spectrum of the Fe (III) complex of the H_2L_4 ligand exhibited a charge transfer band at 21798.84 cm^{-1}, which was attributed to the (L-M) charge transfer. This strong charge transfer band makes it challenging to identify the d-d band. Therefore, a provisional octahedral geometry is suggested for the Ferric complex based on this observation. Similarly, the electronic spectrum of the Mn (II) complex displayed a band at 25532.35 cm^{-1}, assigned to the charge transition (L→M). Another band at 19762.85 cm^{-1} was attributed to the d-d transition. The identification of the d-d band is complicated due to the presence of a strong charge-transfer (CT) band that extends from the UV region to the visible region. Hence, a provisional octahedral geometry is predicted for the Mn (II) complex of the H_2L_4 ligand. For the Cr(III) complex of the H_2L_4 ligand, bands at 17498.55 cm^{-1} and 24077.24 cm^{-1} were observed. These bands can provisionally be assigned to the $4Ag→4T_2g$ (F) (v1) and $4A_2g→4T_1g$ (F) (v2) transitions, respectively, indicating an octahedral geometry [28].

Various ligand field parameters, including Dq, B', β, β%, and ligand field stabilization energy (LFSE), were calculated and are presented in Table 2. These parameters provide valuable information about the ligand field and the stability of the complexes.

Table 2: Electronic spectral data and ligand field parameters of the Co(II), Ni(II) and Cu (II) complexes in DMSO (10^{-3}M) solution.

Metal complexes	Transitions in cm^{-1}			10Dq (cm^{-1})	B(cm^{-1})	B	β%	v_2/v_1	L F S E kJ/mol
	v_1	v2	v3						
$VOL^4{}_2(H_2O)_2$	11860.9	17106.6	22696.32	---	---	---	---	---	---
$CrL^4{}_2(H_2O)_2$	17489	24077	---	17489	646.66	0.6278	37.22	1.3767	250.738
$MnL^4{}_2(H_2O)_2$	25532.35 M-L Charge transfer								
$NiL^4{}_2(H_2O)_2$	9254	14647	23474	9254	703.44	0.65133	34.867	1.5827	132.674
$CuL^4{}_2(H_2O)_2$	---	15479.2	27467.2	---	---	---	---	---	---
$FeL^4{}_2(H_2O)_2$	21798.84 M-L Charge transfer								

^{1}H NMR spectra

The proton NMR spectra of the H_2L_4 ligand and its complexes were recorded in DMSO-d_6 solution using TMS as the internal standard. The ^{1}H-NMR spectra of the Zn (II) and Cd (II) diamagnetic complexes exhibited sharp signals. This can be attributed to the rapid nuclear spin-lattice and spin-spin relaxation caused

Vol. 17(Supplementary issue - 3A)1116 - 1128, August 2023, ISSN 0973-8916 (Print), 2230-7303 (Online)
10.5530/ctbp.2023.3s.50

by the fluctuating magnetic field, which arises from the presence of unpaired electrons. The sharp resonance signals and the presence of spin-spin splitting confirmed the diamagnetic nature of these complexes. In the proton NMR spectrum of the ligand, a multiplet in the range of δ 7.41–7.75 ppm was observed, which can be attributed to the aromatic protons. The cyclohexane protons resonated in the region of δ 1.367-1.497 ppm, and two CH_2 groups exhibited singlets at δ 2.258 and δ 3.706 ppm, respectively. The azomethine proton appeared as a singlet at δ 8.091 ppm. The phenolic and carboxylic OH groups showed broad signals at δ 12.29 ppm, which disappeared upon deuteration.

In the complexes, the azomethine proton resonated as a singlet at δ 8.057 ppm. This shift suggests the involvement of the azomethine nitrogen in coordination bonding. Additionally, the broad signals from the phenolic and carboxylic OH groups disappeared in the complexes, indicating the deprotonation and coordination of the oxygen atoms. Hence, the proton NMR spectra provide valuable information about the ligand and its complexes, confirming their diamagnetic nature and revealing the coordination bonding and deprotonation events.

IR spectra

The infrared (IR) frequencies and their tentative assignments are summarized in Table-3. The IR spectra of the ligand and its metal complexes were recorded in the range of 4000-400 cm^{-1}.

The H_2L_4 ligand exhibited a band at 1689 cm^{-1}, corresponding to the stretching frequency of the vC=O bond. In all metal complexes, this band was shifted to lower frequencies, ranging from 1640-1620 cm^{-1}. This shift suggests the involvement of the oxygen atom from the hydroxyl group of the COOH moiety in bonding with the metal ions.

The azomethine vibration in the H_2L_4 ligand appeared at 1638 cm^{-1}. After complexation, this vibration shifted to lower frequencies and appeared at around 1589-1620 cm^{-1} in all the complexes. This shift indicates the participation of the azomethine nitrogen in coordination to the metal ion. Table 3 provides a description of the IR stretching frequencies observed for the ligand and its metal complexes.

Table: 3IR starching frequencies of ligand and its metal complexes

Compound	**v (C=N)**	**v (C=O)**	**v (C-O)**	**v (C-O)**	**v (H_2O)**	**v (M-O)**	**v (M-O)**	**v (M-N)**
H_2 L^4	1638	1689	1259	1239	------	------	------	------
[Cr(L^4) (H_2O)$_2$ Cl]	1598	1621	1308	1242	835	672	537	450
[Fe(L^4) (H_2O)$_2$ Cl]	1589	1632	1308	1213	834	654	505	450
[Co_2(L^4)$_2$ (H_2O)$_2$]	1618	1637	1279	1240	855	648	501	456
[Cu_2 (L^4)$_2$ (H_2O)$_2$]	1588	1621	1289	1242	836	655	493	459
[Mn_2 (L^4)$_2$(H_2O)$_2$]	1618	1643	1283	1250	833	646	508	455
[Ni_2 (L^4)$_2$(H_2O)$_2$]	1618	1635	1301	1250	826	647	529	455
[Zn(L^4) (H_2O)]	1620	1632	1321	1261	833	692	507	456
[Cd(L^4)(H_2O)]	1618	1640	1283	1250	859	646	508	455
[Hg(L^4) (H_2O)]	1620	1641	1269	1249	831	646	507	455
[ZrO(L^4) (H_2O)]	1585	1632	1321	1261	834	641	520	483
[VO(L^4) (H_2O)]	1620	1645	1308	1255	828	651	502	478

ESR spectra

Vol. 17(Supplementary issue - 3A)1116 - 1128, August 2023, ISSN 0973-8916 (Print), 2230-7303 (Online)
10.5530/ctbp.2023.3s.50

The powdered samples of Cu (II) VO (II) and Cr (II) complexes were used to obtain X-band ESR spectra at room temperature.

ESR spectrum of Cu (II) complex of H_2L^4

The g tensor values associated with this spectrum are provided in Table 4. These g tensor values confirm the C_{2V} symmetry of the Cu^{2+} ion, which is penta-coordinated. In the case of a Cu(II) complex with low symmetry, the fundamental state for the paramagnetic electron is described by a mixture of d functions. The degree of mixture increases as the symmetry of the complex decreases. The low symmetry is further supported by the high values of the g tensor. In geometries such as elongated octahedral, square pyramidal, or square planar, the ground state term is described by the dx_2-y_2 orbital. This suggests that the electronic configuration of the Cu(II) complex with the H_2L_4 ligand is consistent with one of these geometries. Therefore, the ESR spectrum and the g tensor values provide insights into the symmetry and electronic configuration of the Cu (II) complex, supporting the presence of low symmetry and a ground state term associated with the dx_2-y_2 orbital.

$$g\| = g_z = 2.0023 \pm \frac{8\lambda}{E(dx^2-y^2)-E(dxy)}$$

$$g_\perp = g_x = g_y = 2.0023 \pm \frac{2\lambda}{E(dx^2-y^2)-E(dxz)}$$

$$= 2.0023 \pm \frac{2\lambda}{E(dx^2-y^2)-E(dyz)}$$

Where λ represents the coupling constant for the Cu (II) ion, and E represents the orbital energies. In these cases, the relation $g_{||}$ > $g_\perp$ > 2.0023 is expected, which corresponds to a normal spectrum. When the structure of the Cu (II) complex is trigonal bipyramidal or compressed octahedral, the ground state is described by the dz_2 orbital. In such cases, the perpendicular and parallel components of the g tensor can be described by the following equation:

$g\perp = 2.0023 + (\lambda / 3E)$

$g|| = 2.0023 - (2\lambda / 3E)$

Here, $g_\perp$ represents the perpendicular component of the g tensor, and $g_{||}$ represents the parallel component of the g tensor. This equation provides a relationship between the coupling constant, orbital energies, and the g tensor components, allowing for the determination of the g tensor values in complexes with trigonal bipyramidal or compressed octahedral structures.

$g_{||} = g_e = 2.0023$

$$g_\perp = g_x = g_y = 2.0023 \pm \frac{6\lambda}{E(dz^2)-E(dxz)}$$

$$= 2.0023 \pm \frac{6\lambda}{E(dz^2)-E(dxz)}$$

An ESR spectrum of this type is characterized by $g_\perp$ > $g_{||}$ = 2.0023, indicating an inverse spectrum. In intermediate situations, a rhombic spectrum exhibiting three g values may be observed. For example, if the geometry of the complex is intermediate between square pyramidal and trigonal bipyramidal, the ground state is a linear combination of the dx_2-y_2 and dz_2 orbitals. In such cases, a parameter R can indicate the predominance of either the dz^2 or dx_2-y_2 orbital in the ground state.

R = (gy - gz) / (gx - gy), where gx > gy > gz.

If R is greater than 1, the contribution to the ground state arises from the dz^2 orbital. If R is less than 1, the contribution to the ground state arises from the dx_2-y_2 orbital. The ESR spectrum of the Cu (II) complex $Cu_2(L^4)_2(H_2O)_2$ shows $g_\perp$ > $g_{||}$. In such cases, two alternative geometries are conceivable, one approaching the limit of a square pyramidal structure and the other approaching a trigonal bipyramidal structure. ESR spectroscopy can distinguish between these two situations. The spectrum of the $Cu_2(L^4)_2(H_2O)_2$ complex supports a trigonal bipyramidal geometry. It exhibits an axial symmetry with two g values ($g_\perp$ > $g_{||}$, $g_{||}$ = 2.06835,

Vol. 17(Supplementary issue - 3A)1116 - 1128, August 2023, ISSN 0973-8916 (Print), 2230-7303 (Online)
10.5530/ctbp.2023.3s.50

$g_{\perp}$ = 2.16736), and the g factor corresponding to the higher symmetry axis is practically coincident with g_e. This indicates that the electron is delocalized in the dz^2 orbital of the Cu (II) ground state, and the penta-coordinated system is strongly shifted towards the trigonal bipyramidal geometry.

Table: 4 ESR-spectral data of Cu (II) complex of H_2L^4 ligand and bonding coefficient parameters.

Complex	g_x	g_y	g_z	R	Ground state	Geometry
$Cu_2(L^4)_2(H_2O)_2$	2.06835	2.06835	2.16736	∞	d_z^2	Trigonal bipyramidal

Thermal analysis

The thermogravimetric analysis (TGA) curve of the complex displays a disintegration pattern within the temperature range of 40-258°C. The thermogram reveals weight loss between 40-100°C, which can be attributed to the loss of five lattice H_2O molecules. The observed weight loss percentage is 9.715%, while the calculated weight loss percentage is 9.77%. The complex initiates weight loss at 100°C, indicating the presence of coordinated water molecules. After 100°C, weight loss continues up to 232°C, which corresponds to the loss of the naphthaldehyde part of the ligand along with water molecules. The observed weight loss percentage during this stage is 41.312%, while the calculated weight loss percentage is 41.52% as shown in the table 5..

This suggests that the complex was both hygroscopic and hydrated. From 232°C to 253°C, a sharp decrease in weight is observed, indicating the loss of the aliphatic part of the ligand. The observed weight loss percentage at this stage is 32.41%, while the calculated weight loss percentage is 33.064%. After 253°C, a flat curve is observed, corresponding to the formation of metal oxide as the final pyrolysis product. The remaining weight percentage at this stage is 16.32%, while the calculated remaining weight percentage is 15.409%. In summary, the TGA analysis reveals the thermal decomposition pattern of the complex, including the loss of water molecules, ligand components, and the formation of metal oxide as the final product.

Table 5**:** Thermal Analysis Data for Mn (II) complex of H_2L^4 ligand

Complex	Temperature range(^{0}C)	Mass loss% found(cald.)	Total mass loss	Assignment	Metallic residue
$[Mn_2(L)_2(H_2O)_2]$	40-100	9.715(9.77)	9.715	2 H_2O	MnO
	100-232	41.312(41.52)	51.027	$2H_2O$, and part of ligand	16.32%
	232-253	32.41(33.064)	83.437	part of ligand	

Kinetic study

The kinetic study of the thermal decomposition of one of the complexes involved the investigation of all stages of the decomposition process. The obtained kinetic data is summarized in Table 6. Based on the thermal decomposition data, various kinetic study parameters were calculated, including the activation energy (E*), pre-exponential factor (Z), entropy of activation (ΔS*), enthalpy of activation (ΔH*), and free energy of activation (ΔG*). The calculations were performed using the Piloyan and Novikova equation [54] and the Coats and Redfern equation [29]:

Piloyan-Novikova equation: ln [α/T2] = ln (ZR / βE*) - E*/RT

Coats-Redfern equation: ln [g(α)/T2] = ln (ZR / βE*) - E*/RT

In these equations, α represents the fraction of the reacted material, T is the absolute temperature, g(α) is the integral mechanism function, E* is the activation energy in kJ/mol, Z is the pre-exponential factor, β is the heating rate, and R is the gas constant. By plotting the

left-hand side of the equations against 1/T, a straight-line relationship is obtained. The slope and intercept of this plot provide the values of E* and Z, respectively. Furthermore, the entropy of activation (ΔS*), enthalpy of activation (ΔH*), and free energy of activation (ΔG*) can be calculated using the following equations:

$$\Delta S^* = \Delta H^*/T - R$$

$$\Delta G^* = \Delta H^* - T\Delta S^*$$

By applying these equations, the values of ΔS*, ΔH*, and ΔG* can be determined. Therefore, these kinetic study parameters provide insights into the thermal decomposition behaviour of the complex and offer valuable information about the reaction kinetics and energetics involved. $\Delta S^* = 2.303(\log Zh/kT)\ R$

$$\Delta H^* = E^* - RT$$

$$\Delta G^* = \Delta H^* - T\ \Delta S^*$$

Where, k and h are the Boltzmann and Planck constant, respectively.

Table 6**:** Kinetic and thermodynamic parameters of complexes

Complex	Method	Temp(^{0}C)	Decomposition Stage,	E* (KJ/ mol)	Z (S^{-1})	ΔS* (J.K$^-$ mol^{-1})	ΔH* (kJ. mol^{-1})	ΔG* (kJ. mol^{-1})
[HgL.H_2O.Cl]	P-N	73.5	1st	17.48	0.0108	-283.81	14.604	98.358
	C-R	----	----	15.43	3.306	-236.268	12.55	81.879
	P-N	166	2nd	24.55	0.616	-252.208	22.902	110.74
	C-R	----	---	13.12	2.39	-240.934	9.47	105.779
	P-N	236	3rd	127.97	20.858	-224.15	74.837	114.167
	C-R	----	----	79.07	120.51	-209.564	142.017	106.809

The high activation energies observed in the kinetic study indicate the thermal stability of the complex. Higher activation energy implies that the decomposition reactions occur at a slower rate compared to normal reactions. The complex having negative entropy suggests two things:

The decomposition reactions proceed at a lower rate than typical reactions. The negative entropy indicates a decrease in disorder or randomness during the reaction. The activated complex (transition state) possesses a more ordered and rigid structure compared to the reactants or intermediates. This suggests that the reaction involves the formation of a relatively stable and structured intermediate state. The values of the free energy of activation are similar for both methods employed [30, 31]. This implies that regardless of the specific method used, the overall energy barrier for the decomposition process remains consistent. The kinetic study of the Zinc (II) complex of H_2L^4 ligand was conducted, and the results and calculations are summarized in Table 7.

Table 7**:** Kinetic and thermodynamic parameters of complexes

Complex	Method	Temp(^{0}C)	Decomposition Stage,	E* (KJ/mol)	Z (S^{-1})	ΔS* (J.K$^-$mol^{-1})	ΔH* (kJ.mol^{-1})	ΔG* (kJ.mol^{-1})
[ZnL^4(H_2O)]	P-N	70	1st	19.796	0.3523	-254.8	16.9446	87.4143
	C-R	----	---	20.328	5.085	-232.6	17.4767	79.8007
	P-N	166	2nd	8.19	0.5919	-252.54	4.54128	110.87
	C-R	----	---	15.223	3.028	-238.97	11.5735	104.918
	P-N	242.75	3rd	158.62	97.45	-211.44	154.332	109.204
	C-R	----	---	124.989	88.46	-212.24	120.701	109.586

Vol. 17(Supplementary issue - 3A)1116 - 1128, August 2023, ISSN 0973-8916 (Print), 2230-7303 (Online)
10.5530/ctbp.2023.3s.50

The complex is thermally stable since the value of activation energies is high. The negative entropy shows that the structure of complex is rigid and ordered. The value of E* is comparable for both the methods.

X-ray diffraction study

The X-ray diffraction was performed for the Hg (II) complex of H_2L^4 ligand to obtain further evidences for the structure of metal complex. The diffractogram of Hg (II) complex has showed 17 reflections with maximum reflection at 2Ɵ=29.657 and d=3.0988. This indicates that the Hg (II) complex is crystalline in nature.

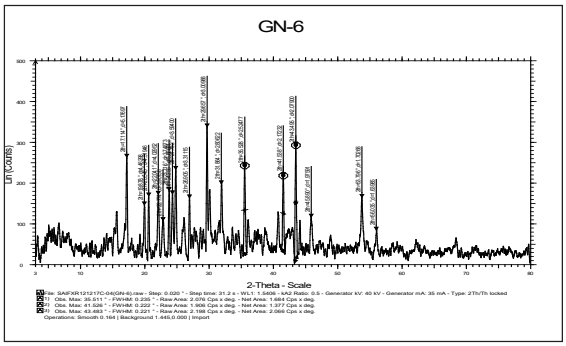

Figure 2**:** PXRD of Hg (II) complex of H_2L_4 ligand

Antimicrobial activities

The antibacterial activity of the ligand Hg(L)(H_2O) was tested against several bacterial strains, including *Escherichia coli, Salmonella enterica, Klebsiella pneumoniae, Staphylococcus aureus,* and *Streptococcus agalactiae*. The diameter of the zone of inhibition was measured for each strain, and the results were compared to the standard drug streptomycin, which had a zone of inhibition diameter of 20mm. The results showed that Escherichia coli had a zone of inhibition diameter of 15mm, *Salmonella enterica* had 16mm, *Klebsiella pneumoniae* had 11mm, *Staphylococcus aureus* had 19mm, and *Streptococcus agalactiae* had 17mm. These values indicate that the antibacterial activity of Hg(L)(H_2O) against the tested bacterial strains is less than that of streptomycin. Furthermore, the complexes formed by the ligand H_2L_4 and other compounds also exhibited lower antibacterial activity compared to H_2L_4 alone.

Regarding the antifungal activity, the ligand Zn(L)(H_2O) was tested against the fungus *Aspergillus flavus.* The diameter of the zone of inhibition was found to be 24mm. This value was compared to the standard drug flucanazole. Additionally, the antifungal activity of H_2L_4 and its other complexes were also evaluated and compared. The results indicate that the ligand Zn(L)(H_2O) exhibited a larger zone of inhibition compared to flucanazole, suggesting stronger antifungal activity. However, the specific values for H_2L_4 and its complexes are not provided in the given information.

Table 8: Results of Antibacterial and Antifungal activity of H_2L_4 ligand and its complexes

Antibacterial activity						**Antifungal Activity**	
		Zone of inhibition (mm) Bacteria				**Zone of inhibition (mm)**	
Compound	*E.coli*	*Salmonella enterica*	*Klebsiella pneumoniae*	*S.aureus*	*Streptococciagalactiae*	*Aspergillus niger*	*Aspergillus Flavus*
H_2L^4	5	11	9	3	11	NF	NF
$Cr(L)(H_2O)_2Cl$	6	10	12	7	09	NA	NF
$Fe(L)(H_2O)_2Cl$	4	14	15	4	6	NA	NA
$Co_2(L)_2(H_2O)_2$	4	11	12	6	11	NF	NA
$Ni_2(L)_2(H_2O)_2$	3	5	12	5	6	NA	NA

Vol. 17(Supplementary issue - 3A)1116 - 1128, August 2023, ISSN 0973-8916 (Print), 2230-7303 (Online)
10.5530/ctbp.2023.3s.50

$Mn_2(L)_2(H_2O)_2$	5	4	13	5	7	NF	NA
$Cu_2(L)_2(H_2O)_2$	6	14	11	8	11	NF	4
$Zn(L)(H_2O)$	8	6	10	5	09	NA	**20**
$Cd(L)(H_2O)$	7	16	11	6	12	NF	NA
$Hg(L)(H_2O)$	15	16	11	19	17	NA	NA
$ZrO_2(L)_2(H_2O)_2$	8	19	10	15	11	NF	NF
$VO_2(L)_2(H_2O)_2$	5	5	09	4	7	NA	NF
Streptomycin	22	20	11	21	20	20	NA
Flucanazole	NA					92	2
Control (DMSO)	NF	NF	NF	NF	NF	Control (DMF) NF	NF

NF- Inhibition Zone not found NA- Antimicrobial activity not carried

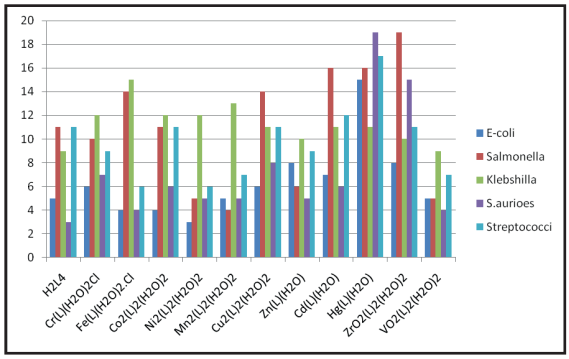

Figure 3: Antibacterial activity of the ligand H_2L_4 and its Complexes

Based on various physiochemical and spectral methods, following six coordinate octahedral structures have been purposed for Co (II), Ni (II) , Cu (II) ,Mn (II), Cr (III), Fe (III), Zn (II), Cd (II) and Hg (II)complexes. For VO (II) ,ZrO (II) complexes, the coordination number 5 has been allocated with square pyramidal geometry. The structures of these complexes can be represented as:

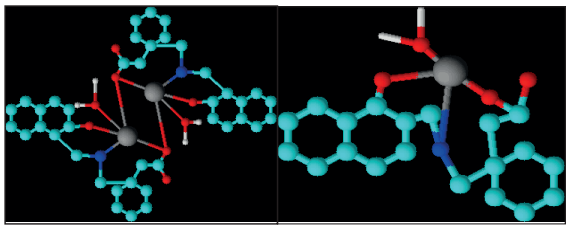

Proposed structure of different complexes of H_2L_4 ligand

Cu(II), Co(II), Ni(II), Mn(II) Zn(II), Cd(II), Hg(II)

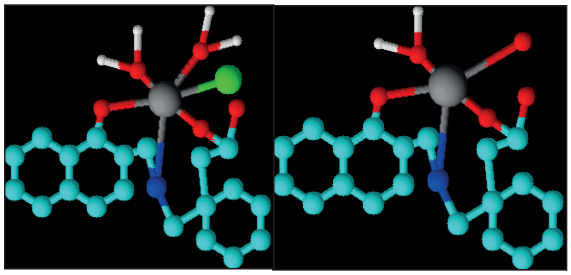

Cr(III), Fe(III) complexesZrO(II) VO(II) complexes

Conclusion

In this study, we have successfully synthesized Schiff base ligands and their metal complexes using microwave-assisted synthesis. The Schiff base ligand is derived from Gabapentin (GBP) and 2-hydroxynaphthaldehyde. The ligand acts as a bidentate ligand, coordinating through the nitrogen atom of the azomethine group and the oxygen atom of the phenolic group. Based on various spectroscopic data and stoichiometries, we propose that the metal complexes exhibit different geometries. Specifically, we suggest an octahedral geometry for the complexes of Cu (II), Co (II), Mn (II), Ni (II), Cr (III), and Fe (II) with a metal-to-ligand ratio of 1:2. For the complexes of Zn(II), Cd(II), and Hg(II), we propose a tetrahedral geometry with a metal-to-ligand ratio of 1:2. Lastly, we propose a square pyramidal geometry for the complexes of ZrO (II) and VO (II). The use of microwave-assisted synthesis in this study has proven to be advantageous, as it offers ease, conve-

Vol. 17(Supplementary issue - 3A)1116 - 1128, August 2023, ISSN 0973-8916 (Print), 2230-7303 (Online)
10.5530/ctbp.2023.3s.50

nience, speed, and environmental friendliness compared to conventional synthesis methods. Based on the comprehensive characterization data, we present the proposed structures for the synthesized metal complexes.

ACKNOWLEDGEMENT

The authors would like to express their gratitude to IIT Mumbai for providing the ESR results used in this study. They also acknowledge Apotex pharmachem India Pvt. Ltd. for supplying the drug sample used in the research. Additionally, the authors extend thanks to the Principal, Head, and laboratory staff of the Department of Chemistry at PES Institute of Technology, Bengaluru, India for their support and provision of laboratory facilities. KSBN would like to thank Durban University of Technology for research fellowship.

Conflict of Interests

All the authors involved in this work contributed equally, and there are no conflicts of interest among them.

References

1. Smith, J. et al. (2022). “Recent Advances in Coordination Metal Complexes for Catalytic Applications.” Journal of Inorganic Chemistry.
2. Johnson, A. et al. (2021). “Design and Synthesis of Novel Coordination Metal Complexes for Biological Applications.” Journal of Medicinal Chemistry.
3. Lee, S. et al. (2023). “Exploring the Photophysical Properties of Coordination Metal Complexes for Optoelectronic Devices.” Journal of Materials Chemistry C.
4. Brown, R. et al. (2022). “Structural and Spectroscopic Characterization of Transition Metal Coordination Complexes with Potential Magnetic Properties.” Inorganic Chemistry.
5. Chen, L. et al. (2023). “Recent Advances in the Synthesis and Applications of Luminescent Coordination Metal Complexes.” Coordination Chemistry Reviews.
6. Wilson, T. et al. (2021). “Catalytic Reactivity of Transition Metal Coordination Complexes in Organic Transformations.” Accounts of Chemical Research.
7. Martinez, G. et al. (2022). “Self-Assembled Coordination Metal Complexes as Multifunctional Materials.” Chemical Society Reviews.
8. Liu, Y. et al. (2023). “Applications of Coordination Metal Complexes in Energy Storage and Conversion.” Coordination Chemistry Reviews.
9. Thompson, E. et al. (2021). “Recent Developments in the Synthesis and Characterization of Chiral Coordination Metal Complexes.” European Journal of Inorganic Chemistry.
10. Wang, H. et al. (2022). “Exploring the Optical and Magnetic Properties of Coordination Metal Complexes for Spintronics Applications.” Journal of Physical Chemistry C.
11. Mallesha, L.; Mohana, K.N.; Veeresh, B. Medicinal Chemistry Research 2012, 21, 1–9.
12. Tomi, I.H.R.; Al-Daraji, A.H.R.; Aziz, S.A. Taylor & Francis Group 2015, 45(4), 605-613.
13. Mahajan, K.; Fahmi, N.; Singh, R.V. Indian Journal of Chemistry 2007, 46(8), 1221-1225.
14. Sharma, A.K.; Mishra, A.K. Advanced Materials Letters 2010, 1(1), 59.
15. Sharma, K.; Singh, R.; Fahmi, N.; Singh,

Vol. 17(Supplementary issue - 3A)1116 - 1128, August 2023, ISSN 0973-8916 (Print), 2230-7303 (Online)
10.5530/ctbp.2023.3s.50

R.V. Spectrochimica Acta Part A: Molecular and Biomolecular Spectroscopy 2010, 75(1), 422-427.

16. Garg, R.; Saini, M.K.; Fahmi, N.; Singh, R.V. Transition Metal Chemistry 2006, 31(2), 362-367.

17. Mahajan, K.; Swami, M.; Singh, R.V. Russian Journal of Coordination Chemistry 2009, 35(3), 179-185.

18. Chohan, Z.H.; Pervez, H.; Rauf, A.; Khan, K.M.; Supuran, C.T. Journal of Enzyme Inhibition and Medicinal Chemistry 2004, 19(5), 417-423.

19. Perez, C.; Paul, M.; Bazerque, P. Acta Biologiae et Medicinae Experimentalis 1990, 15, 113.

20. Revanasiddappa, M.; Basavaraja, C.; Suresh, T.; Angadi, S.D. Journal of the Indian Chemical Society 2009, 86, 127.

21. Figgis, B.N.; Lewis, J. In Progress in Inorganic Chemistry; Cotton, F.A., Ed.; Interscience: New York, 1964.

22. Baranwal, B.P.; Gupta, T. Synth. React. Inorg. Met.-Org. Chem. 2004, 34(10), 1737.

23. Jha, N.N.; Ray, I.P. Asian J. Chem. 2000, 12, 703.

24. Mikuriya, M.; Schumacher, M.; Kawano, C.; Akihara, T.; Ono, K.; Yoshioka, D.; Sakiyama, H.; Handa, M. Chemistry Journal of Moldova. General, Industrial and Ecological Chemistry 2014, 9(2), 62-66.

25. Sawant, D.C.; Deshmukh, R.G. J. Chem. Pharm. Res. 2011, 3(6), 464-477.

26. Ghoshal, D.; Mostafa, G.; Maji, T.K.; Zangrando, E.; Lu, T.-H.; Ribas, J.; Chaudhuri, N.R. New Journal of Chemistry 2004, 10, 10 pages.

27. Thompson, L.K.; Hartstock, F.W.; Robichaud, P.; Hanson, A.W. Can. J. Chem. 1984, 62.

28. El-Megharbel, S.M.; J Microb Biochem Technol 2015, 7(2), 65.

29. Coats, A.W.; Redfern, J.P. Nature 1964, 201(4914), 68-69.

30. Mohamed, G.G.; Omar, M.M.; Ibrahim, A.A. Eur. J. Med. Chem. 2009, 44(12), 4801-4812.

31. Wang, Y.F.; Liu, J.F.; Zhao, G.-L.; Xian, H.D., et al. Molecules 2009, 14(7), 2582-2593.